In-Flight Performance of the Detectors on HST/Wide Field Camera 3

Randy A. Kimble*[a] and the WFC3 Team
[a]NASA's Goddard Space Flight Center, Code 667, Greenbelt, MD USA 20771

ABSTRACT

Wide Field Camera 3 (WFC3)[1,2] is a powerful new imager recently installed on the Hubble Space Telescope during Servicing Mission 4. WFC3 covers wavelengths from the near UV (200nm) to the near infrared (out to 1.7µm), in two channels. The UV/visible (UVIS) channel utilizes two low-noise, UV-enhanced 2K×4K CCD detectors from e2v, while the IR channel incorporates a 1K×1K 1.7µm cutoff HgCdTe array, custom-developed for the WFC3 program by Teledyne[3]. We report here on the performance of the detectors in-flight as observed in the Servicing Mission Orbital Verification program.

1. INTRODUCTION

Wide Field Camera 3 (WFC3) is a general-purpose, broad-band astronomical camera (Figure 1) that was recently installed (May, 2009) into the Hubble Space Telescope (HST) in Servicing Mission 4 (SM4). WFC3 is a facility instrument that was developed by the HST Project on behalf of the astronomical community. Broad scientific guidance for the WFC3 program has been provided by a Scientific Oversight Committee, chaired by Robert O'Connell of the University of Virginia; day-to-day scientific support of the program has been provided by a team of astronomers from the Goddard Space Flight Center and the Space Telescope Science Institute. Development of the hardware was led by Goddard Space Flight Center, with Ball Aerospace as the principal off-site partner, and support from a number of Goddard in-house contractors.

Fig. 1. Wide Field Camera 3 in environmental testing at Goddard Space Flight Center in 2008.

With a broad wavelength coverage in two channels – the UV/visible (UVIS) channel covers 200-1000nm, while the IR channel covers 850-1700nm – WFC3 has been designed to complement the performance of the HST/Advanced Camera for Surveys (ACS), whose Wide Field Channel (WFC) is optimized for deep I-band imaging. WFC3 provides its optimized performance in the near-ultraviolet and near-infrared wavelength octaves bracketing the peak performance region of the ACS/WFC. In these near-UV and near-IR regions, WFC3 provides major increases in the observing power of HST.

*randy.a.kimble@nasa.gov; phone 301-286-5783; fax 301-286-1753

At the time of this conference (October, 2009), WFC3 has completed its Servicing Mission Orbital Verification (SMOV) program and has begun routine scientific observing. This paper provides a snapshot of the in-flight performance of the detectors for WFC3 as characterized by the SMOV program. More detailed, continually updated, information on detector performance as well as all other issues related to the instrument can be found in the Instrument Handbook and Instrument Science Reports ("ISRs") that are linked from the main WFC3 web page at the Space Telescope Science Institute: http://www.stsci.edu/hst/wfc3 .

The detector performance analyses presented here come from the efforts of two teams: 1) The WFC3 team at STScI for analysis of thermal-vacuum test and SMOV program data – in particular Sylvia Baggett, Tiffany Borders, Susana Deustua, Michael Dulude, Bryan Hilbert, John MacKenty, Peter McCullough, and Adam Riess; and 2) the Detector Characterization Laboratory (DCL) at Goddard Space Flight Center for laboratory investigations of WFC3 detector performance – in particular Nicholas Boehm, Nicholas Collins, Greg Delo, Roger Foltz, Robert Hill, Eliot Malumuth, and Augustyn Waczynski. **Most importantly**, the detectors themselves were developed by e2v (CCDs) and Teledyne Imaging Sensors (HgCdTe focal plane array) and packaged for flight by Ball Aerospace.

2. UVIS CHANNEL

2.1 UVIS channel detectors

The heart of the UVIS channel is a focal plane comprised of a mosaic pair of 2K×4K backside-thinned CCD43 arrays (Figure 2), with 15 µm pixels. The CCDs are UV-optimized in their backside surface treatment and AR coating. The UVIS channel covers the 200-1000nm range with a field of view of 160×160 arcsec at a sampling of 0.039 arcsec/pixel; the gap between the two CCDs is ~35 pixels or 1.4 arcsec. Cooling to the nominal operating temperature of -83C is provided by a 4-stage thermoelectric cooler (TEC), whose hot side is connected via gas-charged heat pipe to the instrument's radiator on the anti-sunward side of the HST spacecraft.
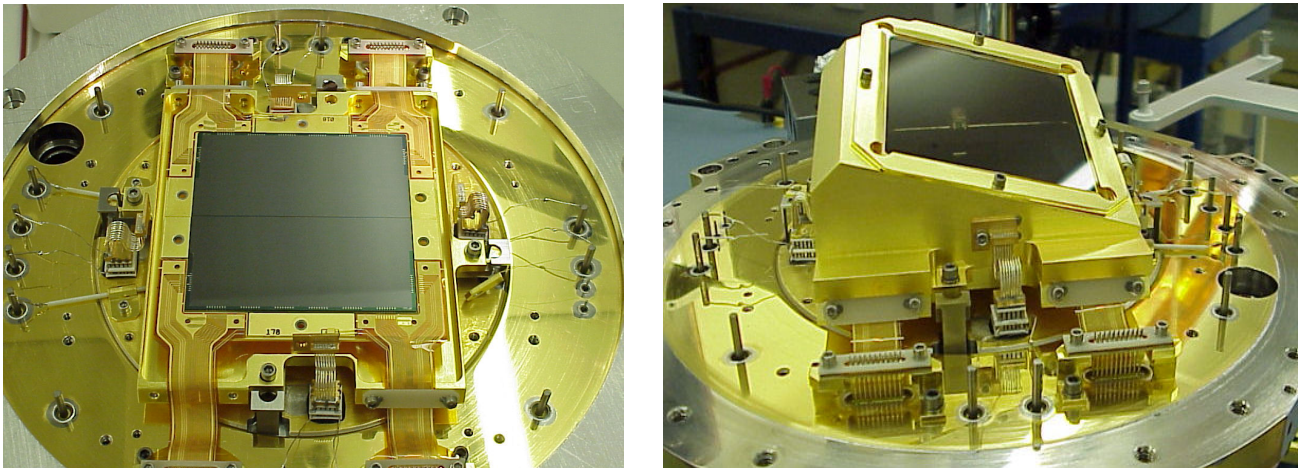

Fig. 2. (left) View of the UVIS channel's CCD focal plane, showing the pair of UV-optimized e2v CCDs. The 4-stage TEC is bonded beneath the CCD carrier and thus is not shown in this view. (right) The UVIS assembly with its inner window assembly (thermal radiation shield). This assembly is cooled to an intermediate temperature of ~ -45C by four 2-stage TECs, reducing the heat load onto the CCD assembly and its 4-stage cooler. The camera head contains an additional cover assembly (not shown) that completes the vacuum housing and provides high-z shielding against the orbital energetic particle environment. This flight CCD package was built by Ball Aerospace.

Full-frame readout of the CCD pair is accomplished through 4 amplifiers at the corners of the focal plane. Subarray readout is available for faster framing of smaller fields of view. Binning modes are available for reduced read noise at coarser pixel sampling. An electronic charge injection capability is available for mitigating the degradation of charge transfer efficiency (CTE) with radiation damage, which is expected to be significant in the later years of the mission. This charge injection capability can provide a high background level of charge over the field (~10 ke-), thus improving CTE, with a much lower noise penalty (~15 e- rms) than the Poisson noise (100 e- rms) of an equivalent signal from a lamp flash. The noise penalty is significant, however, so we do not anticipate use of this feature until some years into the mission.

2.2 UVIS channel science capabilities and early demonstrations

With its UV-optimized CCD efficiency, the UVIS channel of WFC3 is beautifully complementary to the I-band-optimized Wide Field Channel (WFC) of the Advanced Camera for Surveys (ACS), which was successfully repaired during Servicing Mission 4. WFC3 offers a powerful increase in HST capabilities in the near-UV octave of wavelengths from 200-400nm, where it provides a 10-100× increase in survey speed (1/time to survey a given extended field to a given depth) vs. WFPC2 or the High Resolution Channel of ACS (the coverage of the ACS/WFC, with its red-optimized CCDs and silver-coated optics, does not extend to UV wavelengths).

WFC3/UVIS offers a rich complement of narrow-band filters over its full wavelength range. Even for broadband imaging in the red, WFC3/UVIS provides a very capable backup to ACS/WFC, with finer sampling and competitive point-source sensitivity over a 1.6× smaller field of view. The two instruments can also be used very effectively in parallel observations, bringing both of their 16 Mpixel cameras to bear on high-resolution observations of neighboring fields of a target.

A beautiful demonstration of the power of the WFC3/UVIS channel was given in the set of Early Release Observations[4] that were demonstrated to the public in September, 2009. A particularly striking image from the Early Release set is shown in Figure 3.
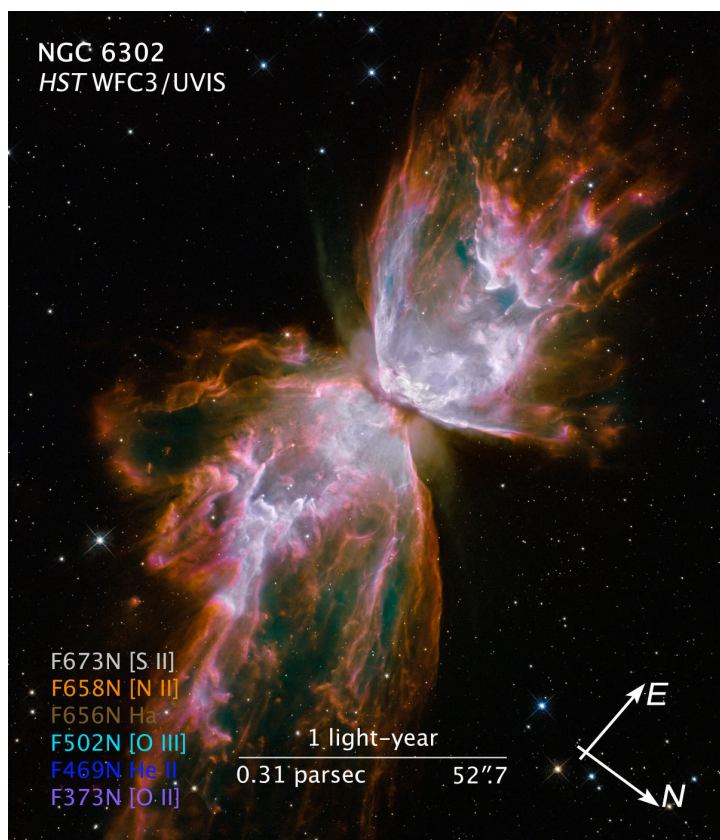

Fig. 3. WFC3 Early Release Observation of the so-called Butterfly Nebula, NGC6302, which demonstrates the sharp angular resolution of the UVIS channel in a rich set of narrowband filters at the wavelengths of key nebular emission lines.

Another striking set of early images with the UVIS channel has been obtained by the WFC3 Science Oversight Committee in their Early Release Science program. The theme of their program is "Star Formation Near and Far"; they are investigating the global processes of star formation, well-resolved in nearby systems, and in integrated properties in galaxies at intermediate redshift. A lovely example of the kind of data they are obtaining on nearby star-forming galaxies is shown in Figure 4. The first publication from this particular observation is an analysis of the population of supernova remnants in the galaxy M83 by Dopita et al.[5]

mature, fully
Superclusters,
dissipated dust

newest
generations
of stars
Forming in
dust lanes

winds from
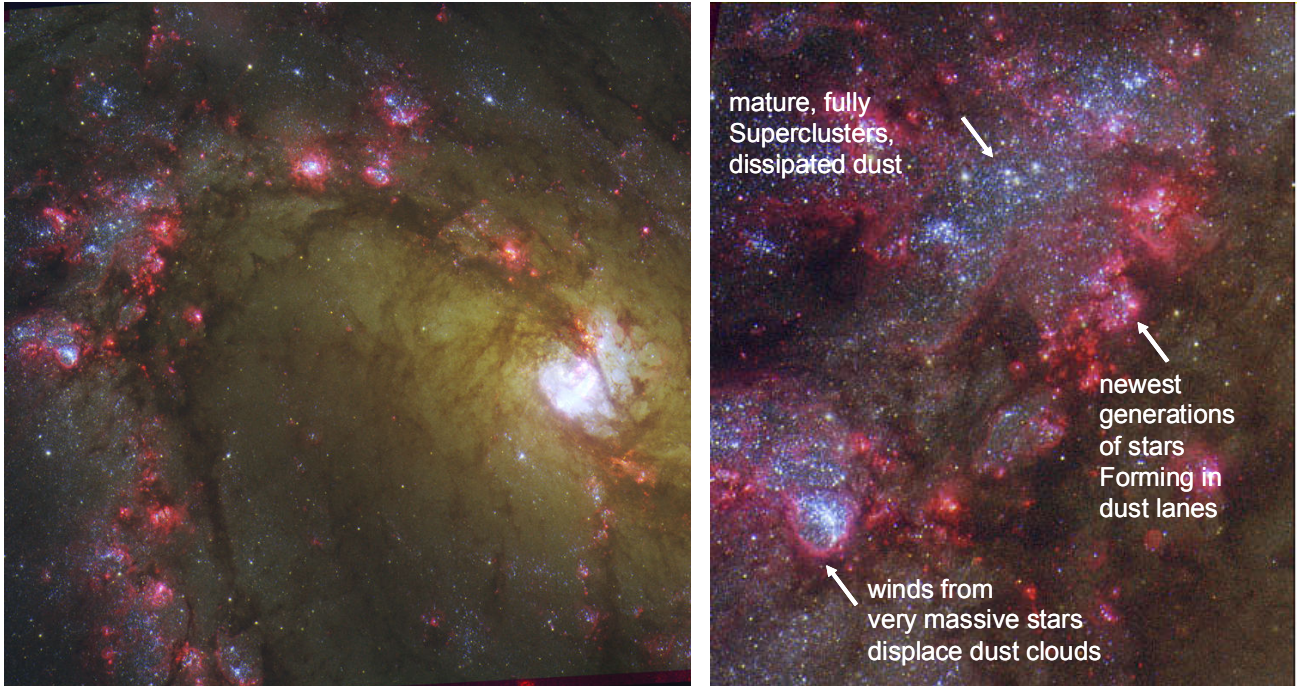very massive stars
displace dust clouds

Fig. 4. (left) WFC3/UVIS image of nucleus and partial spiral arm of the star-forming galaxy M83. (right) Detail showing star clusters at various evolutionary stages.

2.3 UVIS detector performance

The quantum efficiency of the UVIS channel CCDs, as determined in ground test, is shown in Figure 5, which indicates the very high UV QE offered by the devices. Note that the QE plotted here is electrons out per photon in, i.e. it has not been corrected for quantum yield, which is expected to yield >1 electron per detected photon at wavelengths below 340nm. Our statistical analysis of UV flats[6] indicates that the quantum yield in this wavelength range for these devices is quite modest, only 1.10-1.15 down to 200nm, in contrast to the factor of 1.7 expected from the canonical formula of $340/\lambda(nm)$.
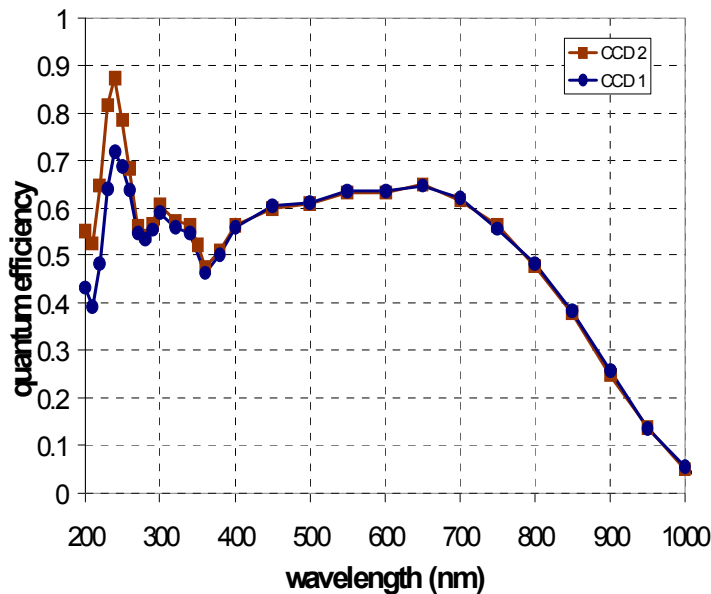

Fig. 5. Quantum efficiency of the CCDs of the WFC3/UVIS channel. Note that the plotted QE has not been corrected for quantum yield at near-UV wavelengths. We have found the quantum yield in this wavelength range to be not much greater than 1, significantly smaller than expected from the canonical formula[6].

A representative UV flat field for one of the flight CCDs is shown in Figure 6. The relatively strong pattern in the flat is a result of the step-and-repeat laser anneal backside surface treatment used by e2v. Visible flat field images on the devices are very smooth.
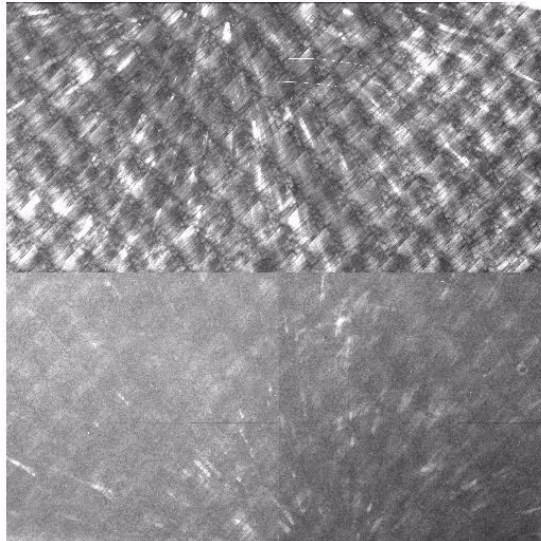

Fig. 6. Flat field image at 336 nm wavelength for one of the flight WFC3/UVIS CCDs.

The read noise and dark current of the CCDs in flight are excellent, as had been seen on the ground. The read noise is ~3.1 e- rms in all four readout amplifiers[7], the lowest of any of the HST CCD imagers. Median dark current runs at <2 e-/pix/hr, higher than the ground rate of only 0.3 e-/pix/hr, but still negligible[8]. The combination of low read noise and low dark current for the CCDs is particularly valuable for WFC3. Because of its very fine sampling (0.039 arcsec/pixel) and significant emphasis on UV and narrowband imaging, sky counts in typical exposures are very low, placing a premium on having a camera with minimum detector noise.

One of the most intriguing behaviors of the WFC3 CCDs encountered in ground test was the occasional appearance of a "bowtie" morphology in some flat-field images, revealed most clearly by ratioing such an image against a nominally identical flat in which the peculiar morphology was not present (Figure 7, left). Further characterization of the behavior provided strong evidence that the bright region of the bowtie represented proper, pinned response of the CCD, while the response of the darker region was improperly low.

A thorough investigation of this strange behavior, using spare CCDs after the flight instrument was delivered for launch processing, was undertaken by GSFC's Detector Characterization Laboratory[9]. Though the particular bowtie morphology was never fully explained, it was found to be clearly related to a subtle QE hysteresis behavior of the CCDs. It was found that when the CCDs are cooled from room temperature *with no illumination*, the response of the CCDs on reaching operating temperature is initially low by 3-5%. A sequence of flat-field exposures is then found to gradually increase the response until it is pinned at a stable value (Figure 7, right). This pinning can be accomplished either by a large number of low-level flats, by a modest number of medium-level flats, or by a single flat of a few hundred thousand electrons.

Unlike many examples of QE hysteresis in CCDs, this behavior was found to be of comparable strength at UV wavelengths as at visible wavelengths, suggesting that the charge-trapping that is presumed to be the cause is not occurring just at the surface. The integrated charge deficit (the total amount of charge "missing" from the low-response flats until stable response is achieved) was found to be ~2000 e-/pixel.

Further laboratory investigation established several crucial aspects of the behavior[9]: 1) visible light (500nm) illumination suffices to pin the response at all wavelengths, including UV, and 2) once pinned, the response is stable for very long periods at the WFC3 operating temperature of -83C, declining only ~0.1% over the course of 10 days (presumably the reason this behavior has not been more commonly recognized – a little bit of illumination during the setup of a camera with these devices completely masks the effect). This combination permitted the development of a straightforward protocol that we anticipated would effectively stabilize the response of the CCDs and thus enable accurate photometry in flight.
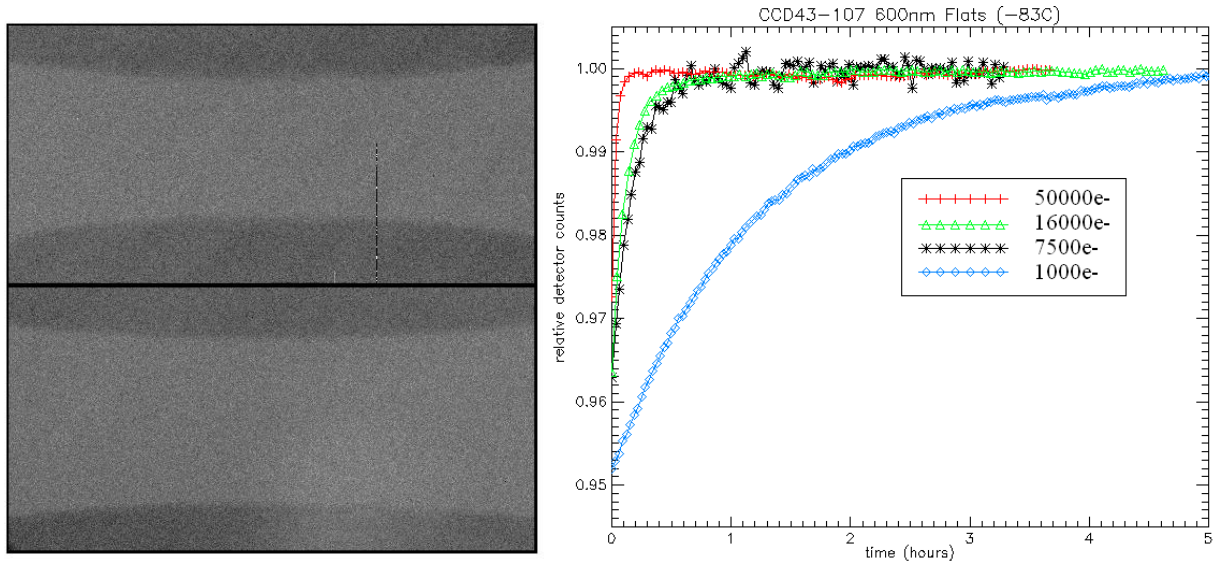
Fig 7. (left) The "bowtie" morphology seen in a small set of ground-test flat-field ratios, indicating unstable QE over at least parts of the detector. (right) Demonstration of the general QE hysteresis phenomenon that was found to be associated with the bowtie behavior. When cooled in the dark, the QE of the CCD starts low, but then gradually increases as the devices receives illumination (in this case, over the course of a sequence of flat-field exposures). The signal delivered per flat is indicated in the figure key, showing how the response is stabilized by several hundred thousands electrons of input signal (see text).

To stabilize the response of the CCDs in flight, we perform the following steps, with a repeat period of no more than a few days:

1) Take a low-level flat to look for any response non-uniformity.

2) Flash the CCDs at a level of 500,000 e-/pixel with ~500nm light, using the onboard calibration system (four tungsten lamps are available for this use).

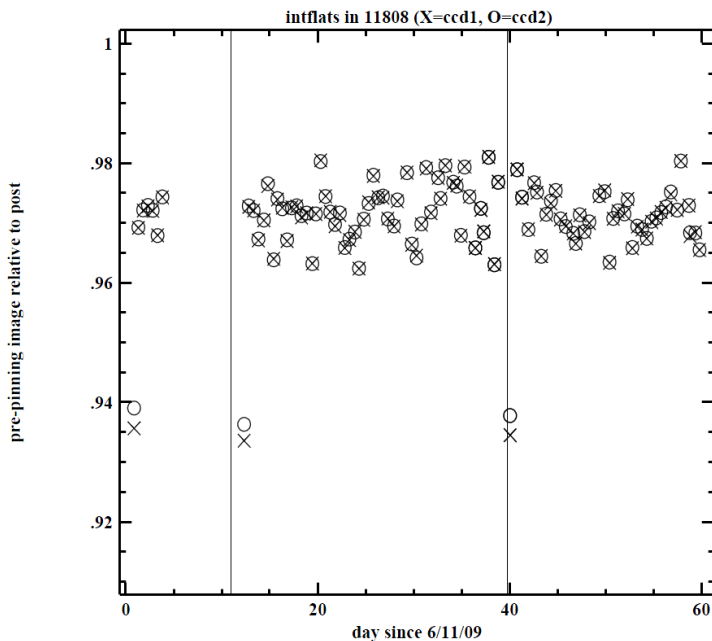3) Take another low-level flat to check again for any response non-uniformity or overall change in level.

Fig. 8. Ratio of the 1st/3rd flat-field signals for the hysteresis-mitigating protocol described above. (× symbols are for one CCD, and the circles are for the other.) The small variation and sub-unity ratio in the general runs is attributed to lamp warmup (see text), while the strong low outliers (down at 0.94), seen *only* after a dark cooldown cycle, are the signature of the hysteresis effect.

The results of repeated runs of this procedure in flight are summarized in Figure 8. We find that during routine operations, the ratio of the 1st to 3rd flat is slightly less than one, but with no spatial structure; the small deficit and scatter in signal level is attributed to warmup of the lamp between the two exposures; evidence for this is provided by the fact that the 1st/3rd ratio is identical for the two CCDs to extraordinarily high precision, which would be expected as a shared response to a slightly increasing lamp brightness, but would be unexpectedly well-matched for the charge-trapping hysteresis behavior. The low outliers in the 1st/3rd ratio are seen *only* when the sequence is run immediately after cooldown after the monthly room temperature anneal. That low ratio (and the off-nominal spatial structure seen in the first flat in only those cases) is the signature of the QE hysteresis effect. The subsequent near-unity ratios with no spatial structure are a signature that the response has been pinned, as confirmed by the excellent repeatability of observations of standard stars with the CCD[10].

Hence, in-flight procedures to ensure that the lamp-flashing protocol is run before resuming observations with the CCD after any warmup (e.g. for the monthly anneals or telescope safing) have proven very effective in enabling stable photometric response for the WFC3 UVIS channel.

As expected, the effects of radiation damage are already being seen in the CCDs. A tail of hot and warm pixels is growing; monthly annealing to the modest temperature of 20C is successful in eliminating a significant fraction of that growth, though of course not all (Figure 9).[11]
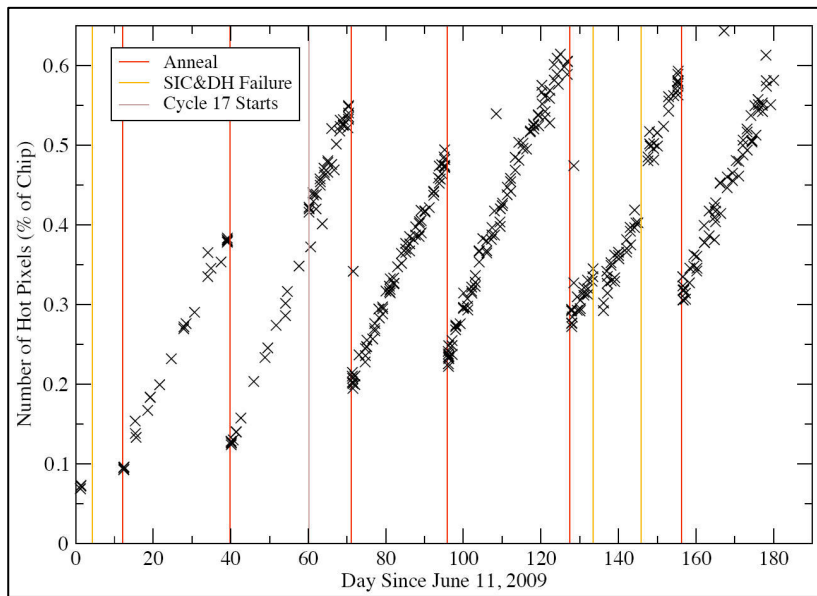

Fig. 9. The growth of hot pixels in flight due to radiation damage. The >80% effectiveness of the monthly anneals is measured by comparing the net growth rate (the slope of the lower boundary of the sawtooth) to the instantaneous growth rate seen between the anneals. The plot was made for a hot pixel threshold of 54 e-/pix/hr.

Charge transfer efficiency is also degrading, on a track that appears to be very similar to what was seen for the very similar ACS/WFC CCDs after launch. CTE degradation is of particular concern for WFC3; as previously noted, much of its use is with UV or narrowband filters that do not provide much CTE-improving background from sky counts. However, we note again the availability of the electronic charge injection mode for mitigation when it becomes appropriate.

In summary, the initial performance of the CCD-based UVIS channel of WFC3 is excellent, and it is actively supporting a rich observing program.

3. IR CHANNEL

3.1 IR channel detector

The heart of the IR channel is a hybrid HgCdTe array from Teledyne Imaging Sensors (Figure 10). The flight device represents the culmination of a custom development program undertaken by Teledyne (then Rockwell Scientific) to provide a HgCdTe array with a 1.7μm long wavelength cutoff. This cutoff wavelength, shorter than had previously been developed for HgCdTe, permits low dark current operation at the relatively modest cooling levels (145K nominal operating temperature) achievable with WFC3's external radiator and thermoelectric cooling, thus requiring no

expendable cryogen or complex mechanical cryocooler. The 1.7μm cutoff also minimizes the response to the thermal background radiation of the HST Optical Telescope Assembly, which operates close to room temperature.
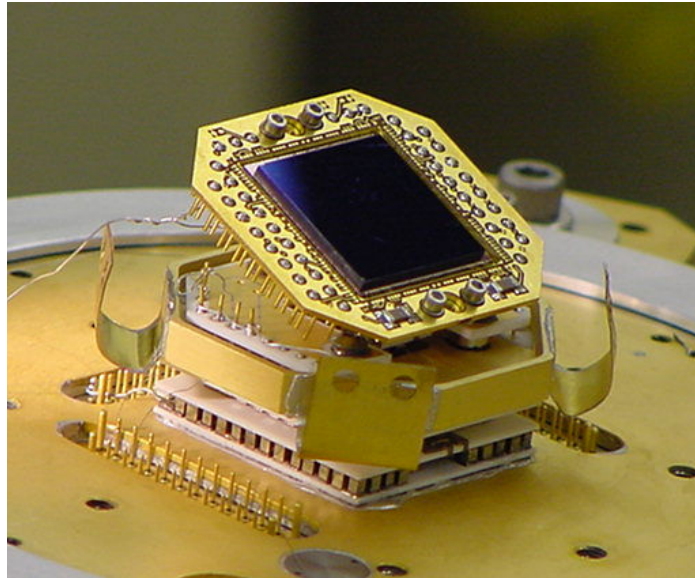

Fig. 10. Flight HgCdTe focal plane array of the WFC3/IR channel, developed by Teledyne Imaging Sensors. The array is shown mounted to a 6-stage thermoelectric cooler in the flight camera head built by Ball Aerospace.

The HgCdTe array is hybridized to a Hawaii-1R mux, providing a 1024×1024 format of 18×18 μm pixels. Of these, 1014×1014 are optically active, with 5 rows and columns of peripheral reference pixels around all edges to help correct for thermal or electrical drifts. The array was grown by the MBE process onto a thick CdZnTe substrate, which was subsequently removed to provided enhanced short wavelength response and to eliminate radiation-induced luminescence of the substrate, which would produce undesirable background signals in the high cosmic ray environment in space[12].

The IR channel covers the 850-1700 nm with a varied complement of broad, medium, and narrow-band filters, as well as two high-throughput, low-resolution grisms. There is no mechanical shutter; exposures are controlled electronically, with readout in the "MULTIACCUM" mode, with up to 16 non-destructive reads per exposure, in a variety of linear, logarithmic, and Fowler-sampled time sequences. All exposures are read out through four off-chip amplifier chains, one for each quadrant.

Development of the custom-cutoff HgCdTe turned out to be quite challenging. By the time of the originally scheduled launch date of Servicing Mission 4, reasonable performance of substrate-on arrays had been achieved, and a flight-quality camera head (IR-2) had been packaged. However, in 2003/2004, the radiation-induced luminescence was discovered, and its source identified as the CdZnTe substrate, in the course of "live" (cold, operating) radiation testing by GSFC's Detector Characterization Laboratory on behalf of the WFC3 program[12].

Fortunately, at that time Rockwell was just learning to remove the substrates from the detectors after growth and hybridization, and the WFC3 program switched to production of substrate-removed HgCdTe arrays[13]. In the early stages of the substrate-removed effort, the fabrications did not yield the desired combination of high quantum efficiency and low dark current; high QE parts typically had high dark current in a significant fraction of the detector pixels (high dark current tail). Due to the proximity of the launch date at the time, one of these devices was nevertheless incorporated into a flight-build camera head (designated IR-1); that unit was in the instrument during one of its major thermal-vacuum test campaigns. With the launch date approaching, "one last lot" of fabrications at (by then) Teledyne was authorized by the HST Project. This last attempt yielded a major leap in performance, with several devices achieving spectacular combinations of QE and dark current. Two of these were successfully packaged by Ball into the final spare and flight camera heads IR-3 and IR-4. The steady performance progression of the IR focal plane arrays and their associated camera heads is shown in Figure 11.
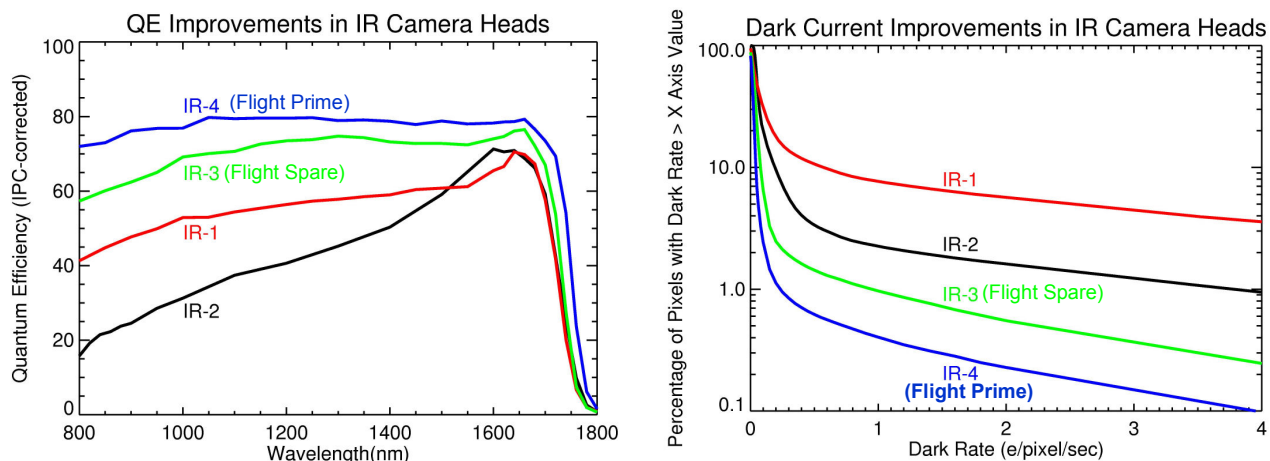
Fig. 11. (left) The performance progression of the WFC3 IR camera head assemblies, showing the increasing quantum efficiency achieved by the FPAs, culminating in the final flight camera head, IR-4. The nearly flat 80% quantum efficiency shown is the proper QE as corrected for the interpixel capacitance effects that distort the gain derived by standard photon-transfer techniques. (right) Cumulative dark current histograms for the same four IR camera heads. What is plotted is the percentage of pixels with dark rate greater than the x-axis value; this highlights the high dark rate tail of the distribution and demonstrates that the final flight and spare camera heads (IR-4 and IR-3) combine high QE with a low percentage of hot pixels.

The culmination of the detector development program was FPA 165 (Figure 12), which was incorporated into camera head IR-4 and selected for flight. That array offered the best combination of QE, dark rate, read noise, persistence, and cosmetics. 96% of its pixels have QE within 10% of the mean. Its cosmetic defects are relatively minor and stable. With fairly tight data quality criteria (low QE, high dark current, unstable behavior from ramp to ramp), 1.8% of the pixels are flagged as "bad" and recommended for deletion from data processing. This modest percentage is readily overcome with a few pointing dither positions in an observing sequence.
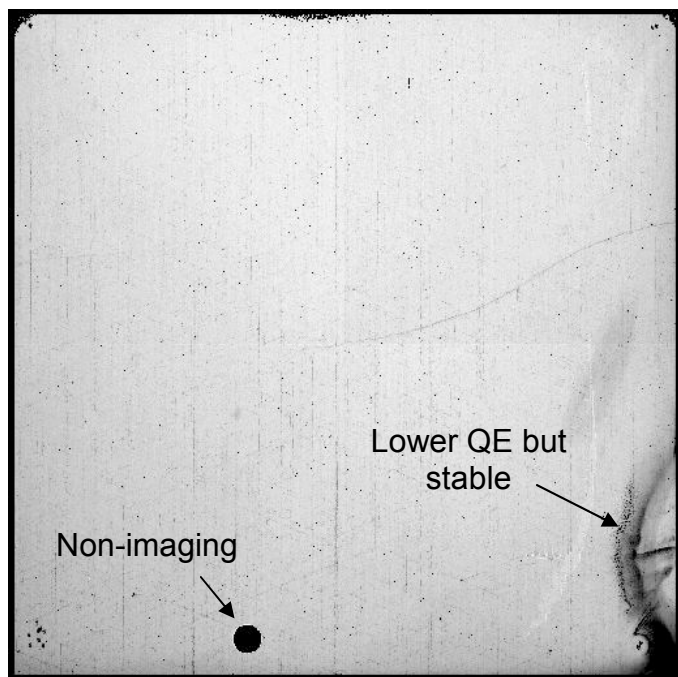

Fig. 12. Flat-field response of flight array FPA 165 at 1400nm wavelength.

3.2 IR channel science capabilities and early demonstrations

The WFC3/IR channel offers higher throughput, 6.4× larger field of view, and 0.130 vs. 0.200 arcsecond sampling vs. the largest field of view camera of NICMOS, the combination yielding a powerful increase in the speed and effectiveness of HST's IR surveys. The requirement on the IR channel was that it have >10× the survey speed of NICMOS; ground calibrations led to pre-flight predictions of >20×. In-flight performance of the IR channel has exceeded that prediction, both in the formal metric calculations of speed (based on throughput, image quality, and detector noise) and in the measured effectiveness against key science goals. Deep imaging with WFC3/IR yields high-redshift galaxy candidates (z > 7) at 40-50× the speed of NICMOS, while accurate photometric observations of Cepheid variables, key to a higher-precision determination of the Hubble constant, also proceed at 30-40× the previous rate.

The Early Release Observations noted above highlighted the performance of the UVIS channel, with its larger imaging format and sharper resolution (due to the finer diffraction limit at shorter wavelengths). However, those images also hinted at the power of the IR channel; the Stephan's Quintet image[4] (Figure 13), though combined with UVIS data in the Early Release image set, showed a striking background of faint, red galaxies detected only or more strongly by the infrared channel, demonstrating its ability to achieve faint detection limits very quickly. This ability has been exploited spectacularly since, with a WFC3/IR image of the Hubble Ultra Deep Field (Figure 14) reaching the faintest detection limits to date for a near-infrared image[14].
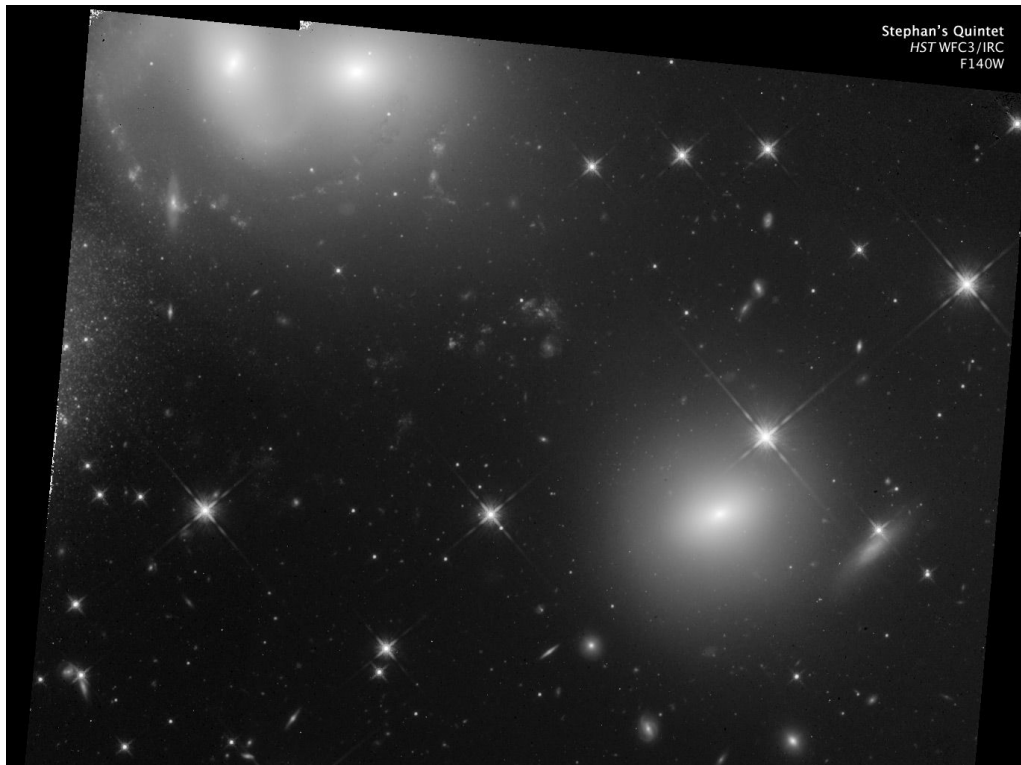

Fig. 13. F140W (1400nm) image of Stephan's Quintet with the WFC3 IR channel. The rich assortment of background galaxies detected in only a few orbits gave an early indication of the striking sensitivity of this channel.
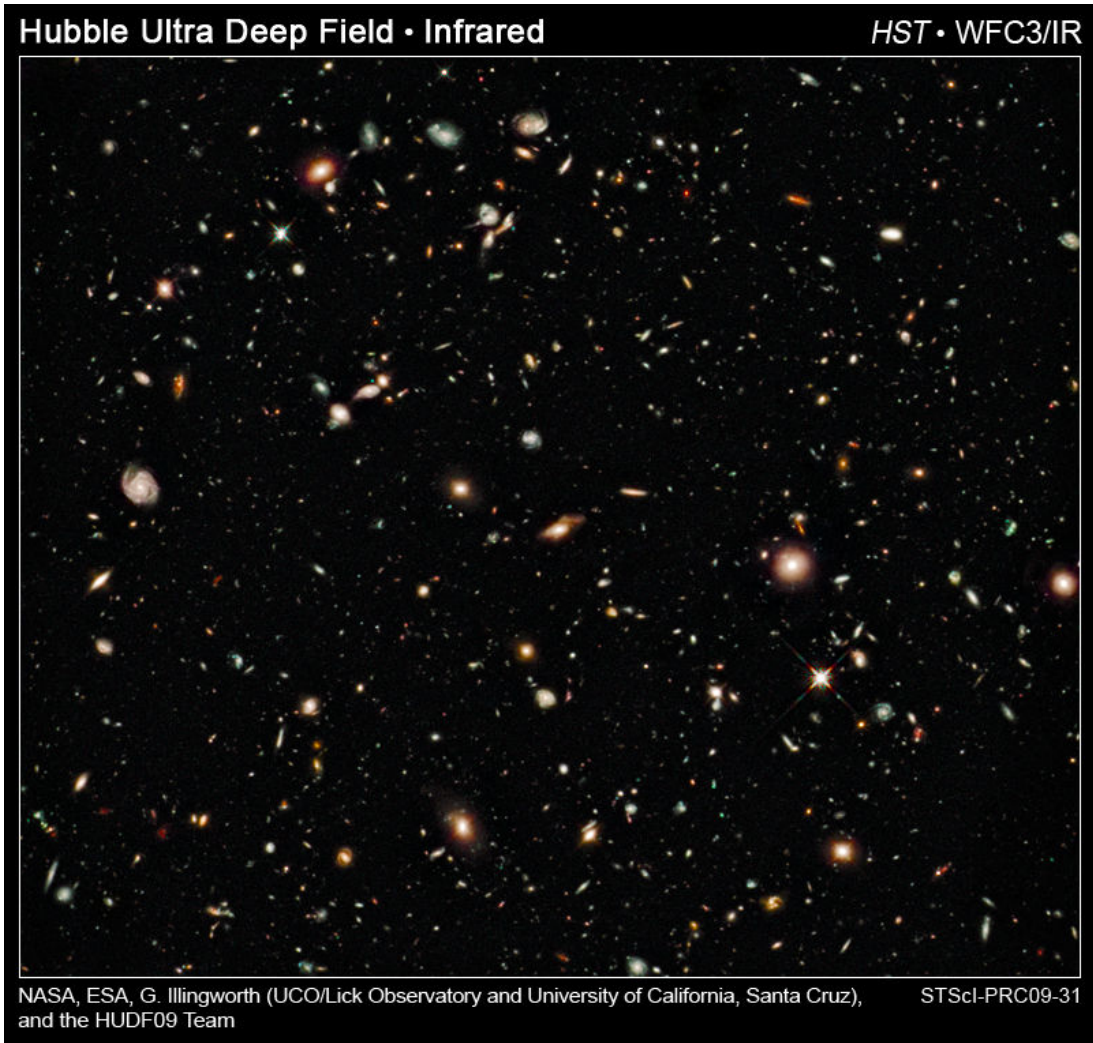
Fig. 14. Color composite image of WFC3's F105W, F140W, and F160W images of the Hubble Ultra Deep Field, taken in ~60 orbits in HST Program 11563 (PI: Garth Illingworth)[14]. This is the deepest near-infrared image of the universe to date, reaching an AB magnitude of ~29. It has been analyzed by several groups who have reported[15-17] an unprecedented number of high-redshift galaxy detections in the range z = 6-9.

3.3 IR detector performance

The performance of the IR detector in flight has been very close to that seen in ground test. Dark current levels and morphology are very similar (Figure 15), with median rates of ~0.048 e-/pix/sec in flight[18] vs. ~0.057 e-/pix/sec in thermal-vacuum test (a potential explanation for the difference is the effects of persistence; in the very busy ground calibration program, the detector was on average exposed to higher signal levels than it is when observing astronomical targets in flight). Only 0.6% of the pixels exceed the dark current specification of 0.4 e-/pix/sec.

Read noise also compares favorably in flight vs. ground test[18]. The CDS read noise is 20-22 e- rms (varies with quadrant); this is the same as the ground result, as is the noise in RAPID readout sequences. The effective noise reading up the ramp for long exposures is actually a bit lower in flight than in thermal-vacuum test, reaching as low as 12.4 e- rms in flight for a full 16-readout exposure with the SPARS200 sequence vs. 14.6 e- rms for a similar sequence in ground test.

The combination of read noise and dark current achieved in flight thus very well satisfies the goal of having the instrument sensitivity be zodiacal-background-limited rather than detector-limited for long exposures in broad-band filters (zodiacal light count rates range from a few tenths to >1 e-/pix/sec).
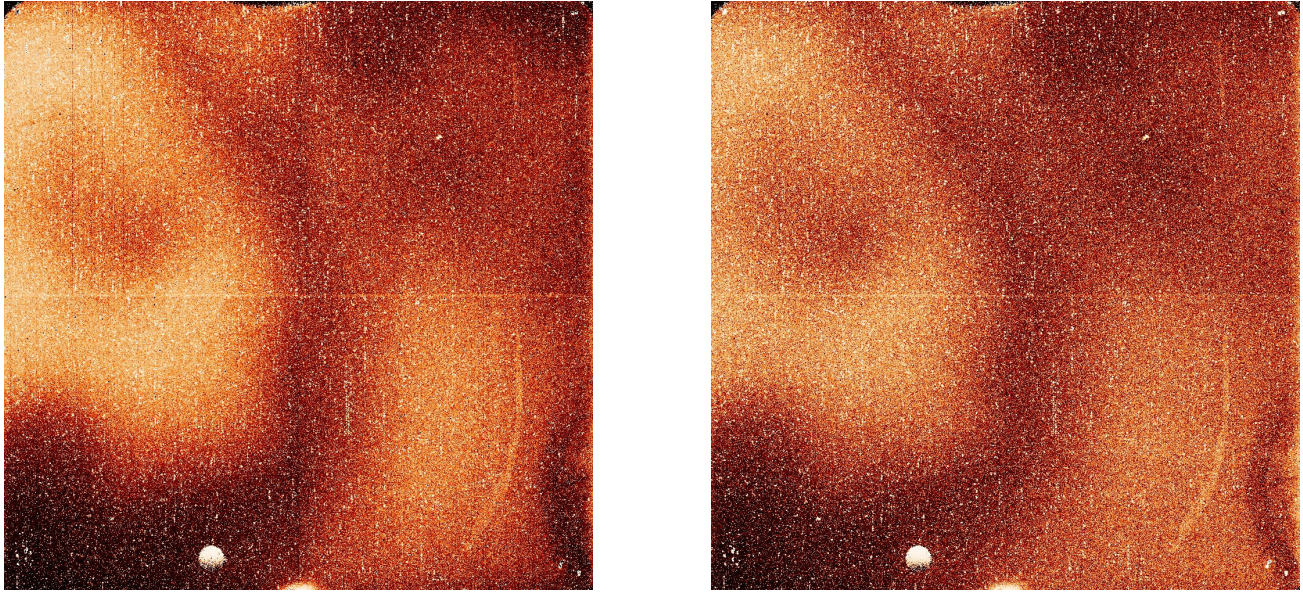
Fig. 15. Dark current images for the WFC3 IR detector in flight (left) and in ground thermal-vacuum test (right).

Image persistence is a common feature of infrared detectors, and it has been particularly prevalent in the development of the 1.7µm cutoff material. The behavior is significant for the WFC3 flight array, and it is an important aspect of observing with the IR channel.

For signals significantly below full well, persistent dark current levels return to within <0.01 e-/pix/sec of baseline in 15-20 minutes (Figure 16), but saturated signals generate persistence effects that can be tracked for hours (Figures 17, 18).
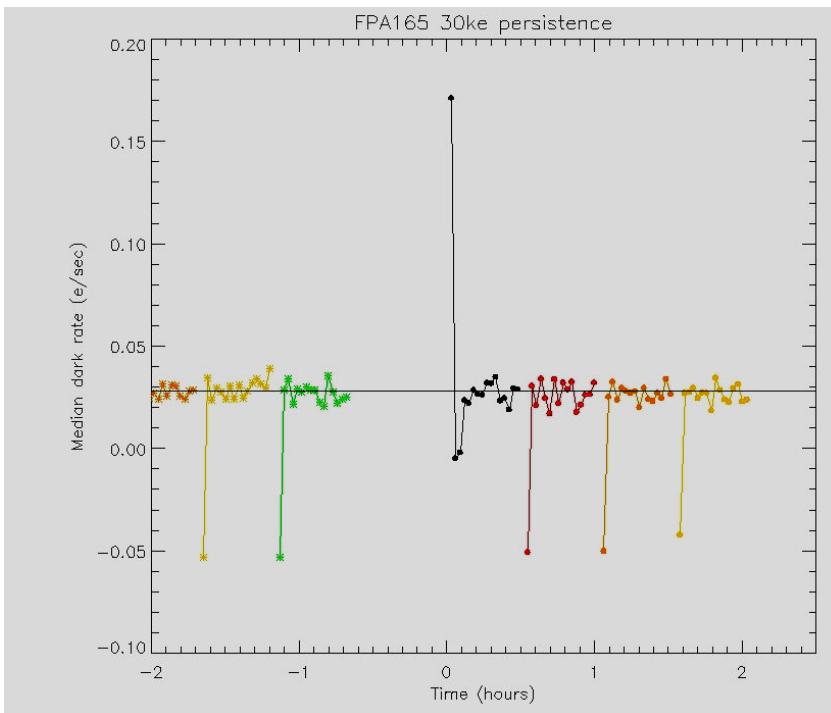

Fig. 16. Persistence response of the flight IR array to a 30 ke-/pixel flat-field input. A sequence of 30 minute 16-read ramps is shown, with the dark rates derived from successive reads within the ramps plotted. The negative rate in the first read difference is a standard reset effect; the positive departure of the first few reads of the dark ramp that began at t = 0 (just after the flat-field exposure) shows the persistence effect; the close agreement of the later reads in that ramp to the corresponding reads in the other darks shows that the persistence has decayed to very low levels within about 15 minutes.

$$Y = 0.156 * (T / 1 \text{ hour})^{-1.00}$$

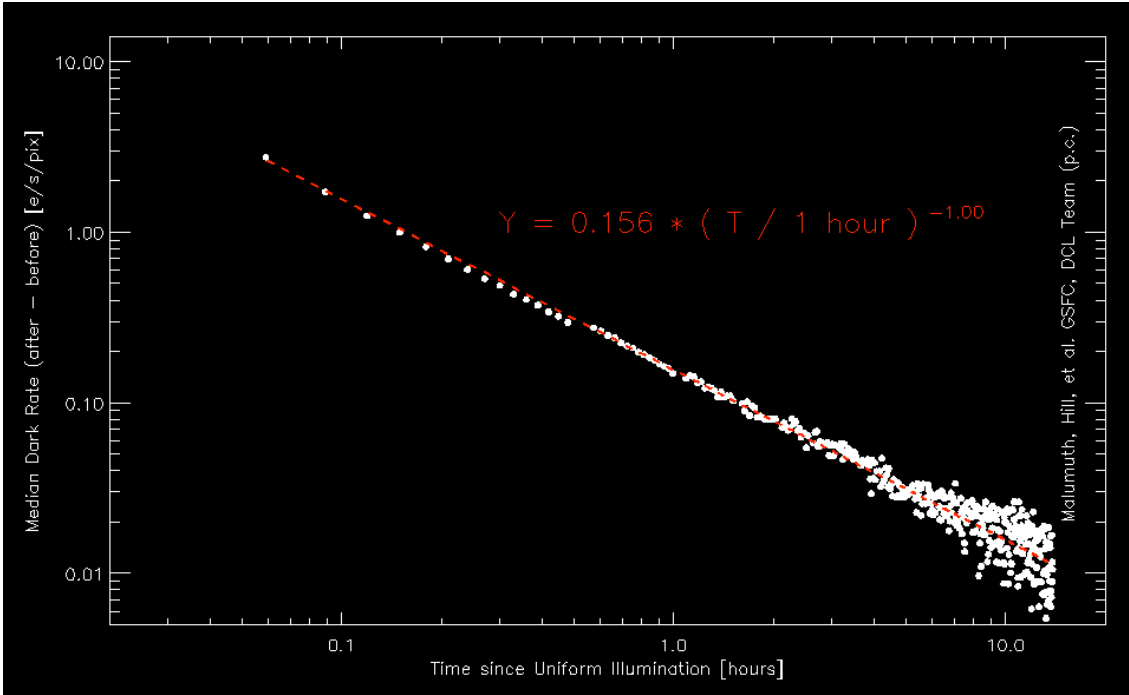Malumuth, Hill, et al. GSFC, DCL Team (p.c.)

Fig. 17. The persistence response to a strongly saturated signal (in this case, 100× full well) can be tracked for hours. This flat-field persistence dark rate measured in ground test is well fit by a power-law going as $t^{-1.0}$; the enhanced dark rate is still detectable above the baseline after 10 hours[19].

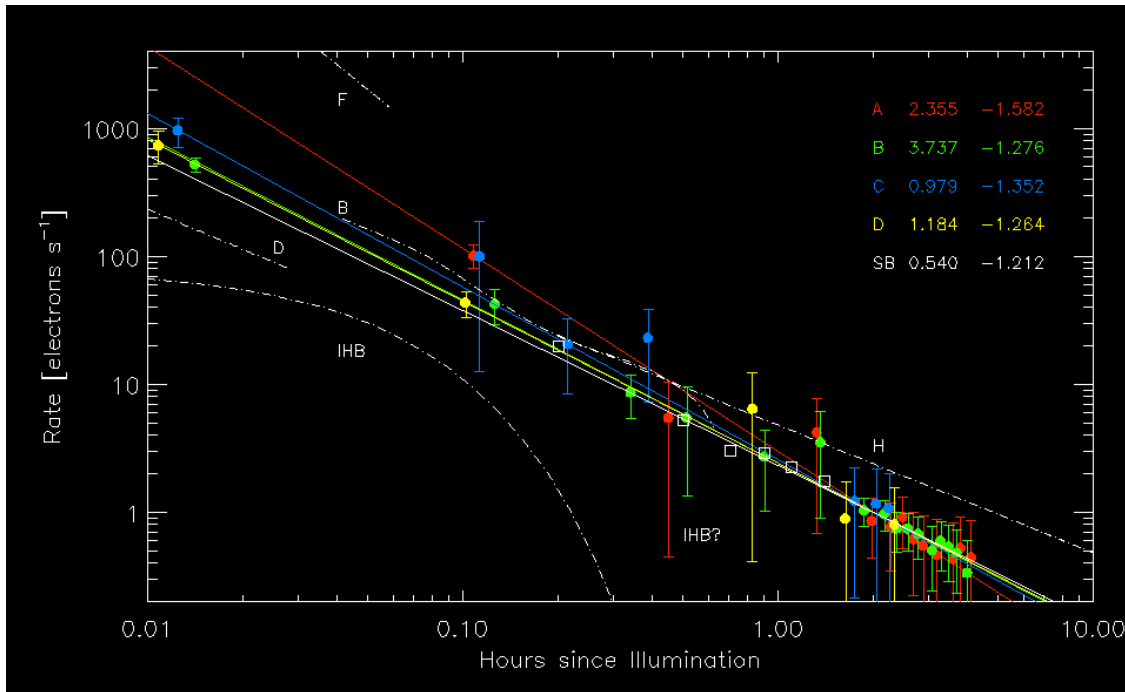|		
A	2.355	−1.582
B	3.737	−1.276
C	0.979	−1.352
D	1.184	−1.264
SB	0.540	−1.212

Fig. 18. For reasons that are not understood, the persistence of small saturated spots decayed more steeply than the persistence from flat fields ($t^{-1.25}$ vs. $t^{-1.0}$), but can still remain detectable for hours[19]. Note that the absolute rates shown here are per arbitrarily sized spot, not per pixel. A reasonable approximation to the persistence from small saturated spots is: $0.15 \times t(hrs)^{-1.25}$ e-/pix/sec.

These persistence effects are likely to be the biggest complication of observing with the WFC3/IR channel. In fact, the first two orbits of the Hubble Ultra Deep Field exposure were severely compromised by persistence from a very bright star cluster than had been observed in the preceding orbits and had to be discarded from the data analysis[15-17].

The ongoing HST Cycle 17 calibration program will better quantify the in-flight persistence behavior of the detector, but it is clear that careful planning of observations will help to mitigate the effects. Dithering is extremely important for separating effects that are fixed in detector space (such as enhanced dark current due to persistence) from real signal (and dithering is clearly beneficial for dealing with the effects of hot pixels and detector cosmetics as well). More darks for tracking the state of the detector would also be useful, within the data storage and transmission limitations of the telescope.

As a further mitigation, STScI has screened the pool of Cycle 17 IR proposals with the Palomar and 2MASS sky surveys to identify particularly bright targets. Over 50% of target fields contain objects that will reach >10× full well in the planned exposures, so general screening against saturated sources is not possible, but the ~10 worst cases of high target brightness have been identified and will be manually scheduled so that they are not followed closely by deep field exposures. An additional mitigation of providing some means of transferring history information between observations is also being investigated. One important point to note in considering the potential persistence effects of an observing sequence is to bear in mind that there is no mechanical shuttering between typical exposures. An opaque position of the relatively slow-moving filter wheel is inserted for slews and passages across the bright earth, but during a sequence of target exposures, the detector is continuously illuminated during readout, filter moves, and small dithers. Hence, the accumulated input to the device can be significantly more than is seen directly in the downlinked exposures.

An additional subtle after-image effect was discovered in the very first external target exposure sequence carried out in flight. A bright galaxy was observed with the IR channel; the core of the galaxy saturated in just a few reads and was thus exposed well above full well by the time the observation was complete. Flat-field exposures taken roughly 30 minutes later showed enhanced response in that saturated region[20] (Figure 19). As the flat-field input rate is relatively high, that excess signal, even though modest in percentage, corresponded to too large a count rate to be accounted for by the additive persistence effects expected for the brightness of the galaxy observed. It appears some form of response hysteresis is operating as well. Closer examination of the readout ramps shows that the greatest percentage excess (up to 2.5%) was seen in reads where the signal had gone above zero-diode-bias (the effective full well condition above which observers are warned that the data are not reliable in any case). However, the effect was still present in earlier, unsaturated, reads, at the sub-1% level.
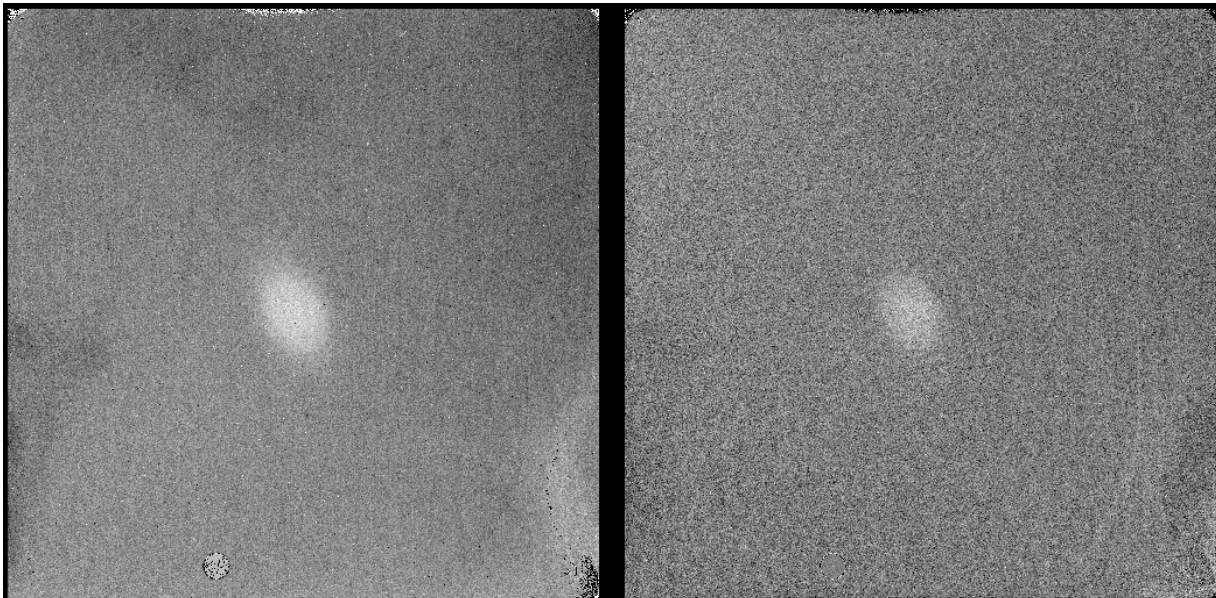

Fig. 19. Ratio of IR channel flat-fields taken ~30 minutes after a bright galaxy exposure to flats taken at other times. Enhanced signal is seen in the region where the galaxy exposure was saturated[20]. The enhanced signal is in excess of that expected from persistence, indicating that there is some form of hysteresis in response as well.

DCL measurements on flight spare FPAs confirm the same basic behavior (Figure 20). The localized response excess in a flat-field taken after a localized over-exposure increases in percentage when the subsequent flat passes zero diode bias (effective full well). However, the excess is still present below full well. After correction for the additive persistence term, the initial excess at sub-full-well signal levels caused by a previous 20× full well exposure was about 0.5%, and the localized excess remained detectable for some hours.
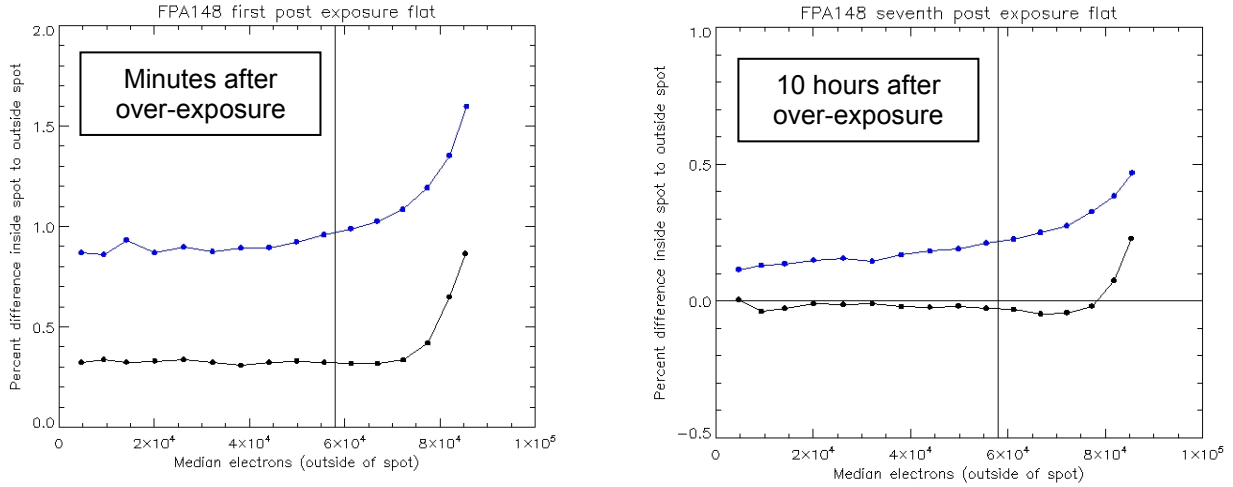

Fig. 20. DCL measurements of the IR hysteresis effect. The plots show the excess response in the region of a localized exposure to 20× full well (blue) and 2× full well (black) over a time span ranging from minutes after the over-exposure (left) to 10 hours after the over-exposure (right). The strong increase in relative response above zero diode bias is apparent, but the initial excess in response is seen down to low signal levels as well. After ten hours, the after-effects of the 2× full well exposure can not be detected (<0.1%), but effects of the 20× full well exposure are still seen.

Another subtle behavior that has been observed for infrared detectors is rate-dependent non-linearity ("reciprocity failure", in the terminology used historically for film). The HST/NICMOS arrays have been shown to exhibit a decreasing response per input photon at decreasing input count rates[21-22]. The effect varies from 3-6%/dex as a function of wavelength, and hence is very significant when one is trying to accurately measure the brightness of a limiting target that is orders of magnitude fainter than the standard stars used for photometric calibration of the instrument. DCL measurements of spare WFC3 devices confirm that the same effect is present in those arrays, though at a lower magnitude; the three parts measured have yielded slopes of 0.3, 0.4, and 1.0 %/dex.
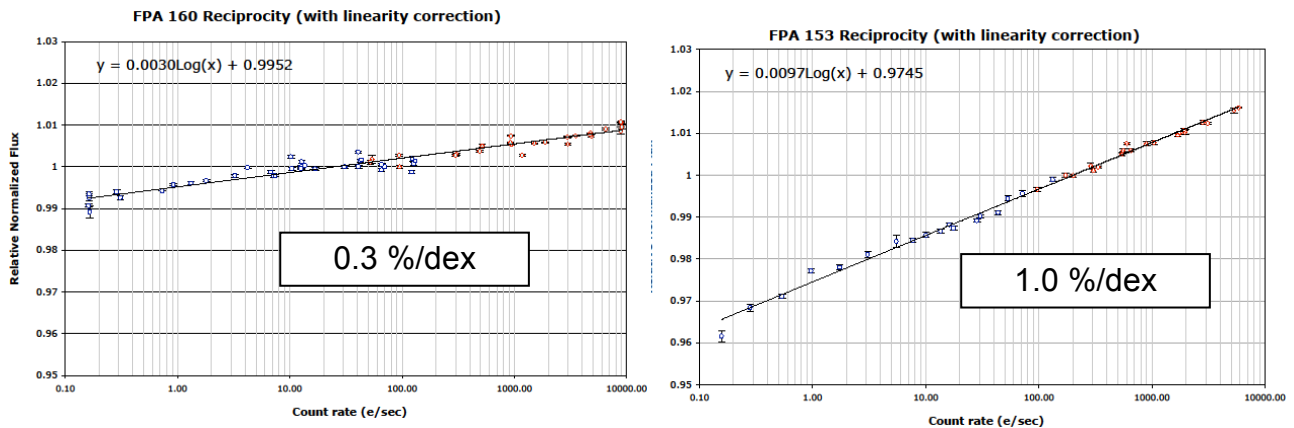

Fig. 21. DCL measurements of reciprocity failure over 5 orders of magnitude of input count rate in two spare WFC3 IR focal plane arrays. Rate-dependent non-linearity is observed with the same sign as seen for the NICMOS arrays (lower response for lower rate inputs), but with much lower slope.

Calibration of this behavior is extremely important for science that depends on deriving accurate absolute brightnesses for the observed targets (such as the critically important use of supernova standard candles to measure dark energy). Adam Riess of STScI has performed an initial calibration of the effect for WFC3/IR by comparing WFC3 photometry with that of NICMOS for stellar fields that have been observed by both instruments. *Under the assumption that the calibration of the rate-dependent non-linearity in NICMOS has been accurately determined*, the implied strength of the effect is ~1.1%/dex for the flight WFC3 array, roughly in the range observed for the spare WFC3 devices in the DCL.

An attempt to measure the effect in WFC3 alone, independent of the NICMOS calibration, will be made in the Cycle 17 calibration program. The approach will be to measure the effects on WFC3 photometry of the same star field when it is observed with varying levels of sky background (achieved by choosing a pointing that skirts the bright earth limb to achieve the varying background rate).

Finally, we have examined the WFC3 in-flight data for the presence of another IR detector behavior that has been observed in ground test by the JWST program. JWST has identified a class of detector events with sudden large signals (above full well, $>>10^5$ e- total) and circular morphologies that they dubbed "snowballs"; the hypothesized source is radioactivity in the detector structure. WFC3 devices show analogous events, typically with smaller diameter, at a generally lower rate than the JWST arrays. Both programs were very interested in the question of whether the rates of such events changed significantly in orbit, though note that DCL measurements showed no increase in snowball rate for devices that underwent total dose radiation testing.

The snowball rate in flight array FPA165 was 0.4-0.7 events/hr on the ground over the full 1Mpixel array. The flight rate appears to be somewhat enhanced (if in fact we are measuring the same phenomenon); excursions up to several events/hr are seen, but with no obviously increasing trend with time[23]. We will continue to track the event rate as the mission proceeds.

At this very low rate, a negligible number of pixels are effected in a given observation, though, since the pixels are saturated in a "snowball", they are rendered unusable for the remainder of the reads in the ramp (as opposed to typical unsaturated cosmic rays, which can be eliminated from a ramp fit while preserving subsequent reads). As saturated events, they do yield the lingering persistence effects noted above.

Though the IR detector exhibits this variety of subtle behaviors – IR arrays are not yet like CCDs – the IR channel's HgCdTe array is similarly performing at a very high level and supporting an extremely exciting observing program.

4. SUMMARY

Wide Field Camera 3, a powerful new imager for the Hubble Space Telescope, was installed into HST during Servicing Mission 4 in May, 2009. Its two imaging channels cover 200-1000nm wavelengths (UVIS channel) and 850-1700nm wavelengths (IR channel). The two channels incorporate, respectively, a UV-optimized pair of e2v CCDs (4K×4K pixels total) and a 1K×1K Teledyne HgCdTe array with a 1.7µm cutoff. The performance of both detectors has been extensively examined over the course of the Servicing Mission Orbital Verification program and has been shown to be highly satisfactory. Utilizing these fine state-of-the-art arrays, WFC3 has begun an extremely productive scientific observing program.

REFERENCES

[1] Kimble, R. A., MacKenty, J. W., O'Connell, R. W., and Townsend, J. A., "Wide Field Camera 3: a powerful new imager for the Hubble Space Telescope," Proc. SPIE 7010, 70101E-70101E-12 (2008).

[2] MacKenty, J. W., Kimble, R. A., O'Connell, R. W., and Townsend, J. A., "Wide Field Camera 3: capabilities and plans for flight operations," Proc. SPIE 7010, 70101F-70101F-9 (2008).

[3] Baggett, S. M., et al., "The Wide-field Camera 3 detectors," Proc. SPIE 7021, 70211Q-70211Q-11 (2008).

[4] "Hubble Opens New Eyes on Universe," STScI News Release 2009-25, http://hubblesite.org/newscenter/archive/releases/2009/25/ (2009).

[5] Dopita, M. A., et al., "Supernova Remnants and the Interstellar Medium of M83: Imaging & Photometry with WFC3 on HST," Ap. J., in press (2009).

[6] Baggett, S., "WFC3 TV3 Testing: Quantum Yield in the UV," WFC3 Instrument Science Report 2008-47, http://www.stsci.edu/hst/wfc/documents/ISRs/ (2008).

[7]   Borders, T., and Baggett S., "WFC3 SMOV Proposals 11419,11426,11431, and 11448: On-Orbit Biases," WFC3 Instrument Science Report 2009-26, http://www.stsci.edu/hst/wfc3/documents/ISRs/ (2009).

[8]   Borders, T., and Baggett S., "WFC3 SMOV Proposals 11419, 11426, 11431, and 11446: On-Orbit Darks," WFC3 Instrument Science Report 2009-16, http://www.stsci.edu/hst/wfc3/documents/ISRs/ (2009).

[9]   Collins, N. R., et al., "Wide Field Camera 3 CCD quantum efficiency hysteresis: characterization and mitigation," Proc. SPIE 7439, 74390B-74390B-12 (2009).

[10]   Kalirai, J. S., et al., "WFC3 SMOV Proposal 11450: The Photometric Performance and Calibration of WFC3/UVIS," WFC3 Instrument Science Report 2009-31, http://www.stsci.edu/hst/wfc3/documents/ISRs/ (2009).

[11]   Borders, T., and Baggett, S., private communication (future Instrument Science Report) (2009).

[12]   Waczynski, A., Marshall, P. W., Marshall, C. J., Foltz, R., Kimble, R. A., Johnson, S. D., and Hill, R. J., "Radiation induced luminescence of the CdZnTe substrate in HgCdTe detectors for WFC3," Proc. SPIE 5902, 161-170 (2005).

[13]   Robberto, M. "FPA#64 and new substrate removed FPAs for WFC3-IR: a tradeoff study," WFC3 Instrument Science Report 2005-19, http://www.stsci.edu/hst/wfc3/documents/ISRs/WFC3-2005-19.pdf (2005).

[14]   "Hubble's Deepest View of Universe Unveils Never-Before-Seen Galaxies," STScI News Release 2009-31, http://hubblesite.org/newscenter/archive/releases/2009/31/ (2009).

[15]   Bouwens, R. J., et al., "Discovery of z~8 Galaxies in the HUDF from ultra-deep WFC3/IR Observations," http://lanl.arxiv.org/abs/0909.1803 , ApJ Letters, in press (2009).

[16]   Oesch, P. A., et al., "z~7 Galaxies in the HUDF: First Epoch WFC3/IR Results," http://lanl.arxiv.org/abs/0909.1806 , ApJ Letters, in press (2009).

[17]   McClure, R. J., et al., "Galaxies at z = 6 - 9 from the WFC3/IR imaging of the HUDF," http://lanl.arxiv.org/abs/0909.2437 , MNRAS, in press (2009).

[18]   Hilbert, B., and McCullough, P. R., "WFC3 SMOV Program 11420: IR Channel Functional Tests," WFC3 Instrument Science Report 2009-23, http://www.stsci.edu/hst/wfc3/documents/ISRs/WFC3-2009-23.pdf (2009).

[19]   McCullough, P. R., and Deustua, S., private communication (draft WFC3 Instrument Science Report 2008-33), (2009).

[20]   Bushouse, H., "WFC3 SMOV Proposal 11421: Channel Select Mechanism Test," WFC3 Instrument Science Report 2009-22, http://www.stsci.edu/hst/wfc3/documents/ISRs/WFC3-2009-22.pdf (2009).

[21]   de Jong, R. S., Bergeron, E., Riess, A., and Bohlin, R., "NICMOS count-rate dependent nonlinearity tests using flatfield lamps," NICMOS Instrument Science Report 2006-001, http://www.stsci.edu/hst/nicmos/documents/isrs/isr_2006_001.pdf (2006).

[22]   de Jong, R. S., "Correcting the NICMOS count-rate dependent non-linearity, " NICMOS Instrument Science Report 2006-003, http://www.stsci.edu/hst/nicmos/documents/isrs/isr_2006_003.pdf (2006).

[23]   Hilbert, B., " 'Snowballs' in the WFC3-IR Channel: Characterization," WFC3 Instrument Science Report 2009-43, http://www.stsci.edu/hst/wfc3/documents/ISRs/WFC3-2009-43.pdf (2009).